Ocean Dynamics (2012) 62:1519–1533
DOI 10.1007/s10236-012-0576-y

Observation-based evaluation of surface wave effects on currents and trajectory forecasts

Johannes Röhrs · Kai Håkon Christensen · Lars Robert Hole · Göran Broström · Magnus Drivdal · Svein Sundby

Received: 23 September 2011 / Accepted: 10 October 2012 / Published online: 9 November 2012

Abstract Knowledge of upper ocean currents is needed for trajectory forecasts and is essential for search and rescue operations and oil spill mitigation. This paper addresses effects of surface waves on ocean currents and drifter trajectories using in situ observations. The data set includes colocated measurements of directional wave spectra from a wave rider buoy, ocean currents measured by acoustic Doppler current profilers (ADCPs), as well as data from two types of tracking buoys that sample the currents at two different depths. The ADCP measures the Eulerian current at one point, as modelled by an ocean general circulation model, while the tracking buoys are advected by the Lagrangian current that includes the wave-induced Stokes drift. Based on our observations, we assess the importance of two different wave effects: (a) forcing of the ocean current by wave-induced surface fluxes and the Coriolis–Stokes force, and (b) advection of surface drifters by wave motion, that is the Stokes drift. Recent theoretical developments provide a framework for including these wave effects in ocean model systems. The order of magnitude of the Stokes drift is the same as the Eulerian current judging from the available data. The wave-induced momentum and turbulent kinetic energy fluxes are estimated and shown to be significant. Similarly, the wave-induced Coriolis–Stokes force is significant over time scales related to the inertial period. Surface drifter trajectories were analysed and could be reproduced using the observations of currents, waves and wind. Waves were found to have a significant contribution to the trajectories, and we conclude that adding wave effects in ocean model systems is likely to increase predictability of surface drifter trajectories. The relative importance of the Stokes drift was twice as large as the direct wind drag for the used surface drifter.

Keywords Wave–current interactions · Trajectory forecasts · Surface drifters · iSphere · Wave effects

Responsible Editor: Arthur Allen

This article is part of the Topical Collection on *Advances in Search and Rescue at Sea*

J. Röhrs (✉) · K. H. Christensen · L. R. Hole · M. Drivdal
Norwegian Meteorological Institute,
Allegaten 70, 5007 Bergen, Norway
e-mail: johannes.rohrs@met.no

G. Broström
Department of Earth Science,
University of Gothenburg,
Gothenburg, Sweden

S. Sundby
Institute of Marine Research,
Nordnesgaten 50, 5005 Bergen, Norway

1 Introduction

The drift velocity of a floating object depends on how it responds to the geophysical forcing represented by the wind, the surface waves, and the ocean currents (Daniel et al. 2002; Breivik and Allen 2008). Operational forecasting centres that provide services for search and rescue need to have access to these physical parameters. Usually, there are three separate numerical model systems for the atmosphere, the surface waves and the ocean circulation, respectively, with various degrees of coupling between the systems.

The response of a floating object to wind can be modelled by assessing the leeway, which is the path relative to the wind (Breivik et al. 2011). The advection by the ocean currents includes parts which are due to the mean drift inherent in surface waves (Stokes 1847) and also the mean currents forced by the waves (Longuet-Higgins 1953). Several approaches exist to account for these wave effects, but, in many cases, they are fully parameterized using only wind speed and direction, hence removing the need for a separate wave model. Such parametrisations implicitly assume that the waves are always correlated with the local wind, something which is often not the case. In this paper, we will focus on the benefit of having a dedicated wave forecasting system in the context of trajectory forecasts.

Taking wave effects into account for ocean and trajectory models has been an effort during the recent years. First approaches parametrise turbulent fluxes from waves to the current (Craig and Banner 1994) using the wind speed. Carniel et al. (2009) use this approach to model surface trajectories. Other studies (Broström et al. 2008; Jenkins 1989) discuss the purpose of numerical wave models to calculate momentum and energy fluxes between waves and the current. An application of the approach by Jenkins (1989) to surface drifters was made by Perrie et al. (2003) and Tang et al. (2007). Observations that relate waves effects to drifter trajectories are rare, but, for example, Ardhuin et al. (2009) estimates the current as well as the wave motion using HF radar data.

This study presents in situ measurement of waves, currents and drifter trajectories. We focus on open ocean conditions, hence we do not discuss near-shore or shallow water dynamics. We discuss the benefits of having coupled model systems, in particular coupled wave and ocean models. The most common approach today is to have a split, one-way coupling for the air–sea momentum and energy fluxes: the wind forces both the waves and the ocean circulation, and there is no coupling between the wave and the mean currents.

We use data collected during a research cruise in April 2011. The data set contains observations from drifting buoys, acoustic Doppler current profilers (ADCPs), and directional wave buoy, as well as ship-based measurements of wind speed and direction. In contrast to previous drifter studies (Perrie et al. 2003; Carniel et al. 2009), which only consider one type of drifting buoy, we deployed two types that sample the currents at different depths. Furthermore, the direct wave measurements enable us to make good estimates of the Stokes drift, and the wave dependent fluxes and body forces.

The outline of the paper is as follows: In Section 2, we give a theoretical introduction on drifter dynamics and wave–current interactions. The measurement location and the instrumentation is described in Section 3, and in Section 4, we summarise the observations. Section 5 is devoted to the evaluation of the various wave effects and analysis of the drifter data. Finally, Section 6 contains some concluding remarks.

2 Theoretical aspects

2.1 Dynamics of a drifting object

The equation of motion for a drifting object with mass m and drifter position $\mathbf{x}$ can be written (Breivik and Allen 2008; Daniel et al. 2002):

$$m\frac{\mathrm{d}^2\mathbf{x}}{\mathrm{d}t^2} = \mathbf{F}_\mathrm{C} + \mathbf{F}_a + \mathbf{F}_o + \mathbf{F}_w, \tag{1}$$

where $\mathbf{F}_\mathrm{C}$ is the Coriolis force, $\mathbf{F}_a$ the wind drag, and $\mathbf{F}_o$ the water drag. The force $\mathbf{F}_w$ is the force due to scattering of waves. Our drifter buoys are small compared to typical wavelengths, and the latter force will be ignored here. Wind and water drag can be expressed by the relative velocity of the drifter to the respective medium (O'Donnell et al. 1997). For instance, the water side drag force for small objects is

$$\mathbf{F}_o = \frac{1}{2}\rho_w A_w C_w \left|\mathbf{u}_\mathrm{L} - \frac{\mathrm{d}\mathbf{x}}{\mathrm{d}t}\right| \left(\mathbf{u}_\mathrm{L} - \frac{\mathrm{d}\mathbf{x}}{\mathrm{d}t}\right). \tag{2}$$

Here, ρ_w is the water density, A_w the effective area that is exposed to the water, C_w a drag coefficient and $\mathbf{u}_\mathrm{L}$ the Lagrangian (particle following) current in the water.

2.2 Modelling mean currents and waves

Equation 2 requires the knowledge of ocean currents. Most numerical ocean circulation models use an Eulerian description of the motion and the currents from such models will be denoted by $\mathbf{u}_E$. A significant part of the upper ocean drift velocities is due to the Stokes drift, which is the intrinsic forward motion associated with surface gravity waves (Stokes 1847). In a wave, the fluid particles describe near closed orbits, but they travel slightly further forward beneath the wave crest compared to the backward motion beneath the trough. This difference results in a net forward transport in the wave propagation direction. This the direct effect of waves on drifting objects.

The Stokes drift is a Lagrangian quantity (i.e., particle following), which means that it cannot be represented in conventional ocean circulation models that use an Eulerian description (e.g. Broström et al. 2008).

The Stokes drift will here be denoted $\mathbf{u}_S$. It is defined as the difference between the Lagrangian and Eulerian velocities and it is customary to write (e.g. Craik 1982)

$$\mathbf{u}_L = \mathbf{u}_E + \mathbf{u}_S. \tag{3}$$

From numerical wave prediction models, we can obtain reliable forecasts of the directional wave spectra, which give complete information about the Stokes drift $\mathbf{u}_S$. These models are based on a statistical description of the sea surface height, in which the waves are represented by a two-dimensional variance spectrum E. We define the wave frequency ω, the wave number $\mathbf{k}$ and propagation direction θ. Introducing the unit vector $\mathbf{i}_k = \mathbf{k}/|\mathbf{k}|$, the phase and group velocities of the waves are $\mathbf{c}_p = (\omega/|\mathbf{k}|)\mathbf{i}_k$ and $\mathbf{c}_g = \partial\omega/\partial\mathbf{k}$, respectively.

The wave models solve the action balance equation, which evolves the spectrum forwards in time according to the source terms S_i (Komen et al. 1994). A simplified version of this equation, suitable for deep-water waves and assuming negligible current refraction, is

$$\left(\frac{\partial}{\partial t} + \mathbf{c}_g \cdot \nabla\right) E = S_{\text{in}} + S_{\text{nl}} + S_{\text{dis}}, \tag{4}$$

where S_{in} represents wave growth due to the action of the wind, S_{dis} wave dissipation due to breaking/white capping, S_{nl} nonlinear wave–wave interactions that distribute energy between the different wave components. The nonlinear interaction term only redistributes momentum and energy between the different wave components, which means that the integral of S_{nl} over all wave components is zero.

Correct to the second order in the wave steepness, the Stokes drift can be written as (e.g. Jenkins 1989)

$$\mathbf{u}_S = 2\int_0^{2\pi}\int_0^{\infty} E\omega\mathbf{k}\exp(2|\mathbf{k}|z)\mathrm{d}\omega\mathrm{d}\theta, \tag{5}$$

In Eq. 5, we have used the fact that deep-water waves decay exponentially with depth. The magnitude and vertical shear of the Stokes drift crucially depends on the wave conditions: young wind sea with predominantly short waves has a Stokes drift with high surface speeds and strong vertical shear, while long period swell is associated with a Stokes drift that is much more uniformly distributed with depth.

2.3 Wave-induced forcing of the Eulerian mean currents

An important point to make here is that the Eulerian mean current $\mathbf{u}_E$ will not be unaffected by the waves. On the contrary, it will be influenced by wave dependent air–sea fluxes of momentum and energy and by wave-induced body forces. We will briefly describe some of the more well-known wave effects and point out some physical inconsistencies that appear when these effects are ignored.

A significant part of the total atmospheric momentum and energy fluxes goes into the wave field. When the waves dissipate, e.g., through wave breaking/white capping, there is a flux of momentum and turbulent kinetic energy from the waves to the ocean. The momentum flux is manifested as a surface (or near surface) stress that accelerates the mean flow (Longuet-Higgins 1953; Weber 1983; Jenkins 1989; Weber et al. 2006), while the energy flux cause enhanced near surface turbulent mixing (Craig and Banner 1994). In the absence of any wave dissipation, the momentum and energy contained in the wave field is simply advected by the waves at the wave group velocity. The wave field should therefore be regarded as a reservoir of mean momentum and energy.

In the simplest coupled system, the wave model acts as a filter between the atmosphere and the ocean, adjusting the air–sea fluxes according to the wave energy budgets. The wave-induced momentum and energy fluxes can be calculated from the source terms in Eq. 1, for example, the momentum flux τ_o into the ocean is (Saetra et al. 2007)

$$\tau_o = \tau_a - \rho_w g \int_0^{2\pi}\int_0^{\infty} \frac{\mathbf{k}}{\omega}(S_{\text{in}} + S_{\text{dis}})\mathrm{d}\omega\mathrm{d}\theta, \tag{6}$$

where τ_a is the total atmospheric momentum flux. The total atmospheric flux is, in general, sea state-dependent (Janssen 1989), but is often calculated from the wind speed and direction using bulk flux formulae (e.g. Smith 1988). From Eqs. 4 and 6, we see that whenever the source terms are unbalanced and the wave field is changing, there is a corresponding change in the effective momentum flux to the ocean.

As an example of the importance of Eq. 6, consider a situation with growing waves. The momentum in the waves, and hence the Stokes drift velocity, then increases. The integral in Eq. 6 will be positive and the effective momentum flux $\boldsymbol{\tau}_o$ to the mean Eulerian currents will be smaller than $\boldsymbol{\tau}_a$. If we force our ocean model with the total flux $\boldsymbol{\tau}_a$ and neglect the wave effects, the Eulerian current will be overestimated. If we then add the Stokes drift and the Eulerian mean currents to obtain the Lagrangian current, we see that the same momentum increase appears twice: first as an increase in the Stokes drift and second as an increase in the Eulerian mean currents. Thus, adding the Stokes drift to ocean model currents without accounting for the wave-induced fluxes violates the fundamental physical principle of momentum conservation and is detrimental for the current predictions.

Similarly, the energy flux from the atmosphere to the waves can be expressed in terms of the input source function

$$\Phi_{aw} = \rho_w g \int_0^{2\pi} \int_0^{\infty} S_{\mathrm{in}} \mathrm{d}\omega \mathrm{d}\theta, \tag{7}$$

while the energy flux from the waves to the ocean can be expressed as

$$\Phi_{wo} = \rho_w g \int_0^{2\pi} \int_0^{\infty} S_{\mathrm{dis}} \mathrm{d}\omega \mathrm{d}\theta. \tag{8}$$

This flux is a result of wave breaking/white-capping and wave–turbulence interactions and increases the turbulent kinetic energy (TKE) in the upper layer of the ocean (e.g. Rascle and Ardhuin 2009). Defining the total atmospheric energy flux Φ_a, we can write an analogue to Eq. 6 for the flux Φ_o into the ocean as

$$\Phi_o = \Phi_a - \rho_w g \int_0^{2\pi} \int_0^{\infty} (S_{\mathrm{in}} + S_{\mathrm{dis}}) \mathrm{d}\omega \mathrm{d}\theta. \tag{9}$$

The direct flux of TKE from the air flow to the ocean is usually considered to be small compared to the other terms (Phillips 1977).

Wave–mean current interactions have been studied for a long time in the context of weakly nonlinear theory. These interactions can be broadly divided in two categories: (a) large scale dissipative or non-dissipative wave, mean-flow interactions and Coriolis forces and (b) small scale dispersion and mixing due to nonlinear instability mechanisms. Large scale here means spatial and temporal scales much larger than the wavelength and period of the waves. Processes in the first category will typically be modelled as wave dependent forcing terms in the ocean circulation models. As an example, one can consider the radiation stresses induced by breaking swell in the near-shore (Longuet-Higgins and Stewart 1964; Weber et al. 2009). In deep water, the dominating contributions are the wave-dependent air–sea fluxes and the so-called Coriolis–Stokes force ($\mathbf{f}_{\mathrm{CS}}$) (Polton et al. 2005; Weber et al. 2008). This latter force is simply the contribution to the Coriolis force from the Stokes drift:

$$\mathbf{f}_{\mathrm{CS}} = -\rho_w f \mathbf{k} \times \mathbf{u}_{\mathrm{S}}, \tag{10}$$

where f is the Coriolis parameter and $\mathbf{k}$ is the unit vector pointing upwards.

Processes that belong to the second category include wave–turbulence-mean flow interactions and small scale circulations such as Langmuir turbulence (Craik and Leibovich 1976; Grant and Belcher 2009). These processes will not be addressed in this paper.

3 Field campaign

The field campaign took place in northern Norway on April 8–13 in 2011. The Institute of Marine Research in Bergen, Norway, has yearly research cruises in the Vestfjorden area during the spawning season of the Atlantic Cod, which raises a particular interest in oceanic conditions in this area.

3.1 Measurement site

Vestfjorden in northern Norway is a wide triangular formed ocean bay bounded along the southeast by a highly mountainous roughed coast intercepted by branched deep fjords (Fig. 1). On the other side, in the northwest, it is bounded by the Lofoten archipelago, another roughed mountain chain intercepted by shallow tidal sounds towards the outer part of the coast. The length of the ocean bay from the head to the mouth is about 180 km, and the width at the mouth is 70 km. The bottom topography is though similar to a real fjord with a deep basin extending down to 700-m depth towards the head and a sill depth of 220 m near the mouth.

The main part of the Norwegian Coastal Current is passing by the mouth of Vestfjorden. A smaller fraction is turning into Vestfjorden flowing in along the southeast side and out in a narrower band (Roed 1980) along the Lofoten Archipelago. The surrounding mountain topography exerts strong influence on the atmospheric circulation above the fjord (Sundby 1982; Jones et al. 1997).

While the flow along the mountain borders on each side of Vestfjorden is rather unidirectional, the central part of the system is dominated by eddies of various sizes (Michelson-Jacob and Sundby 2001). The largest eddies, about 50 km in diameter, occur in the outer

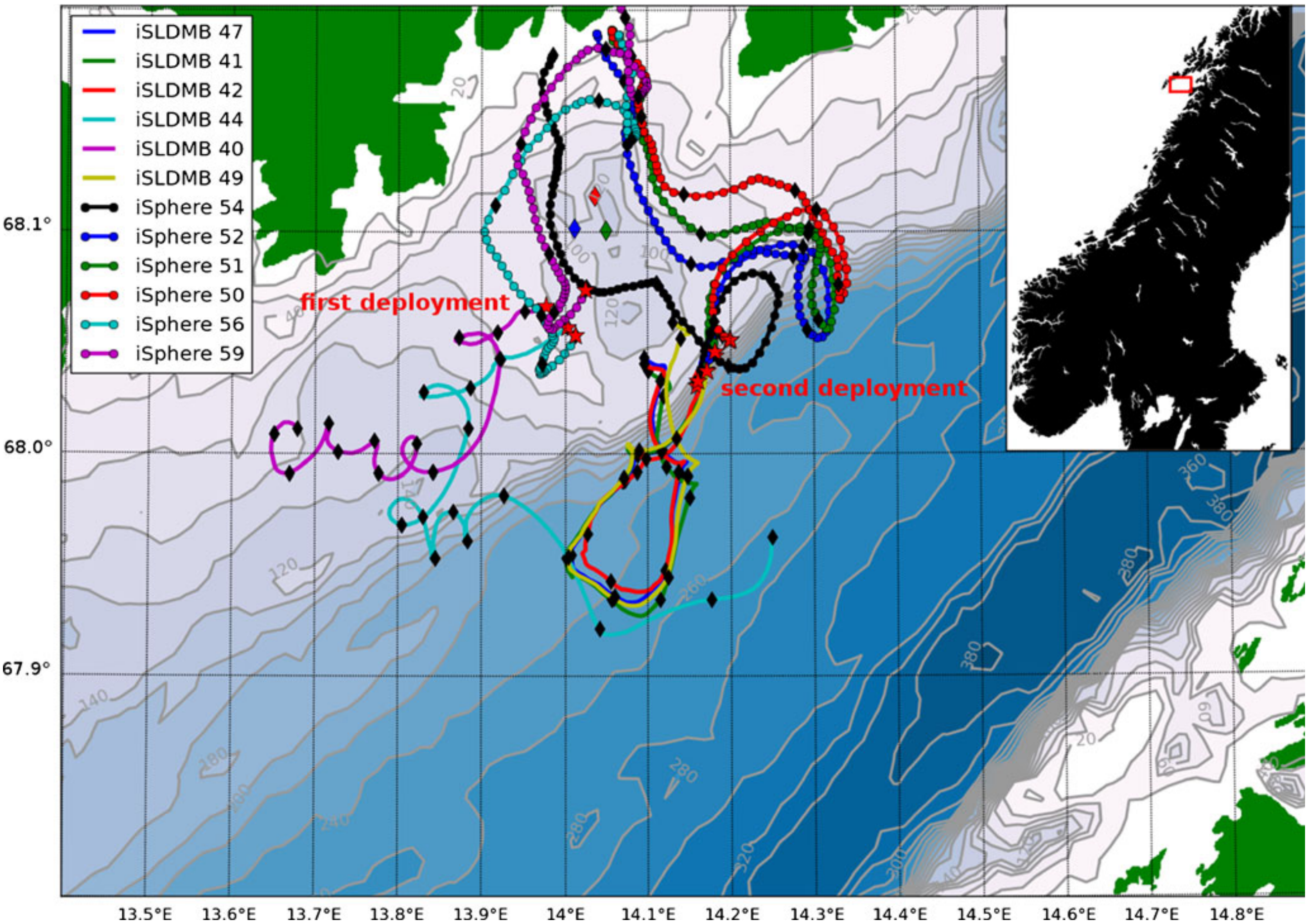

Fig. 1 Drifter trajectories in the Vestfjorden bay at the coast of Nordland, Norway. The *inlet* map shows the location of Vestfjorden in Norway. Bathymetry contours are shown with 20-m intervals and *blue shading*. Mooring stations during the BioWave Cruise 2011 are shown by *coloured markers*, the three stations are arranged as a *triangle* with about a kilometre distance to another with following instruments: *blue dot*, ADCP mooring; *green dot*, wave rider mooring. Trajectories of SLDMB and iSphere drifters until April 12 at 0000 hours are shown in *colours*. Deployment times for each drifter are shown in Table 1, initial positions are marked by *red stars*. *Black diamonds* indicate full 6-h steps (0000, 0600, 1200 and 1800 hours UTC). The SLDMBs (*solid lines*) perform a southwesterly motion with clockwise turning loops. The iSpheres (*dotted lines*) that were launched during the first deployment start with a southwesterly motion before they turn northwards, while the iSpheres that were launched during the second deployment start with a northerly motion followed by a anticyclonic loop

parts of the bay near the sill and are generally anticyclonic. The smaller eddies towards the head are about 20 km in diameter and less. These are generally cyclonic. The observed eddies are generally extending throughout the mixed layer depth which may vary during spring between 50 and 150 m.

Three different moorings were deployed during the cruise. They were positioned approximately 2 km apart forming a triangle. The first mooring contained two ADCPs, the second was the wave rider buoy and the third an experimental buoy for measuring oceanic turbulence. The locations of these moorings are shown in Fig. 1. The research vessel made short excursions from the moorings but was mostly on station in the middle of the triangle.

3.2 Wind measurements

This experiment was carried out with the research vessel “Johan Hjort” of the Institute of Marine Research. A wind vane from the Norwegian Meteorological Institute is installed on this vessel at approximately 19.5 m high above sea level. On April 9 at 1800 hours and April 11 at 1600 hours, the vessel stayed within 5 km of the measurement site, providing wind speed and direction for the presented analysis.

3.3 Directional wave rider buoy

Wave measurements were taken with a Datawell DWR-MkII directional wave rider buoy (Datawell

2007). Vertical and horizontal accelerations along with orientation were measured to yield heave and lateral displacements. The wave buoy measures waves with periods ranging from 1.6 to 30 s and heave with a resolution of 0.01 m within a range of −20 to 20 m at a sampling frequency of 1.28 Hz. The output from the wave buoy are the power spectral density $E(f_n)$ and the mean wave direction ϕ_n for each discrete wave frequency f_n. Such spectra are produced every half hour. The wave rider was deployed during the period April 9 at 1122 hours to April 12 at 1722 hours at the position shown in Fig. 1 (green marker).

3.4 Ocean currents

Oceanic current velocities during the experiment in Vestfjorden were observed using ADCPs. While these instruments measure vertical profiles of the Eulerian velocities, the drifters described in Section 3.5 allow to assess Lagrangian velocities.

Two ADCPs were used, one at 12-m depth and one at the bottom, both looking upwards. The ocean depth at this place is 121 m. The ADCP at the surface is a 1-MHz Nortek Aquadopp ADCP. It recorded 2-min averages of velocities in 25-cm-large vertical bins. Data of the two uppermost wet bins and four bins in 7–8-m depth had to be disregarded due to surface backscattering and ringing effects. The bottom ADCP at 118-m depth is a 190-kHz Nortek Aquadopp ADCP. It records 2-min averages in 2-m bins.

The high signal frequency of the upper ADCP allows to sample high vertical resolution profiles of the upper mixed layer, giving a particular opportunity to study surface processes. We used the bottom ADCP with low resolution and high measurement range to cover the column underneath the upper ADCP.

ADCP data bins were mapped to depth levels for each time step. The data bin intersecting the sea surface is recognised by a maximum of backscatter amplitude. Valid data from ADCP 1 is available between the depths of 0.5 and 10 m. Valid data of ADCP 2 reaches from the depths of 15–115 m.

All ADCP data were low-pass-filtered with a Godin-type time filter over 15 data points, which removes signals with periods of less than 30 min (Emery and Thomson 1997). We applied an additional vertical filter to all upper ADCP profiles because the low size of the bins (25 cm) caused noisy velocity estimates. Much of that noise was reduced by a weighted average filter over three bins, where the centre bin had twice the weight of the adjacent bins.

3.5 Drifting buoys

Two types of surface drifters were deployed during the BioWave Cruise. Six CODE-type (self-locating datum marker buoy (SLDMB) from MetOcean, Canada) drifters were used. These drifters follow the current at approximately 1-m depth and are not directly affected by wind (Davis 1985a). They consist of a cross-shaped sail extending from 0.3- to 1.2-m depth underneath the surface with small floats at the surface.

We also deployed six surface drifters (iSpheres from MetOcean). These are spheric floats with a diameter of 35 cm, being half-submerged in water and therefore exposed to the wind. They have an aerodynamically smooth shape, and previous studies indicate that this type of drifter shows similar behaviour as crude oil (Aamo and Jensen 1997). Their main use is for oil spill tracking (Belore et al. 2011).

Both drifter types transmit their positions over the Iridium satellite network. SLDMB drifter positions are reported every 10 min, while iSphere positions are reported every 30 min. The SLDMBs drifters stayed in the interior parts of Vestfjorden for more than a week, while all the iSpheres stranded after a few days during a strong wind event. Deployment times are listed in Table 1.

4 Meteorological and oceanographic conditions

4.1 Wind and waves

The weather situation during the period of interest was dominated by passing low pressure systems; on April 9 at 0000 hours, there was a low pressure system located between Norway and Spitsbergen, which gave westerly winds over Lofoten. This low pressure moved northwards, and a new low pressure system

Table 1 Drifter deployment times in UTC

SLDMB drifter	40	41	42	44	47	49
Deployment time	9.4. 17:20	10.4. 10:27	10.4. 11:12	9.4. 16:47	10.4. 10:57	10.4. 10:43
iSphere drifter	50	51	52	54	56	59
Deployment time	10.4. 10:27	10.4. 10:43	10.4. 10:57	10.4.11:12	9.4. 16:47	9.4. 17:20

Deployment positions are marked in Fig. 1

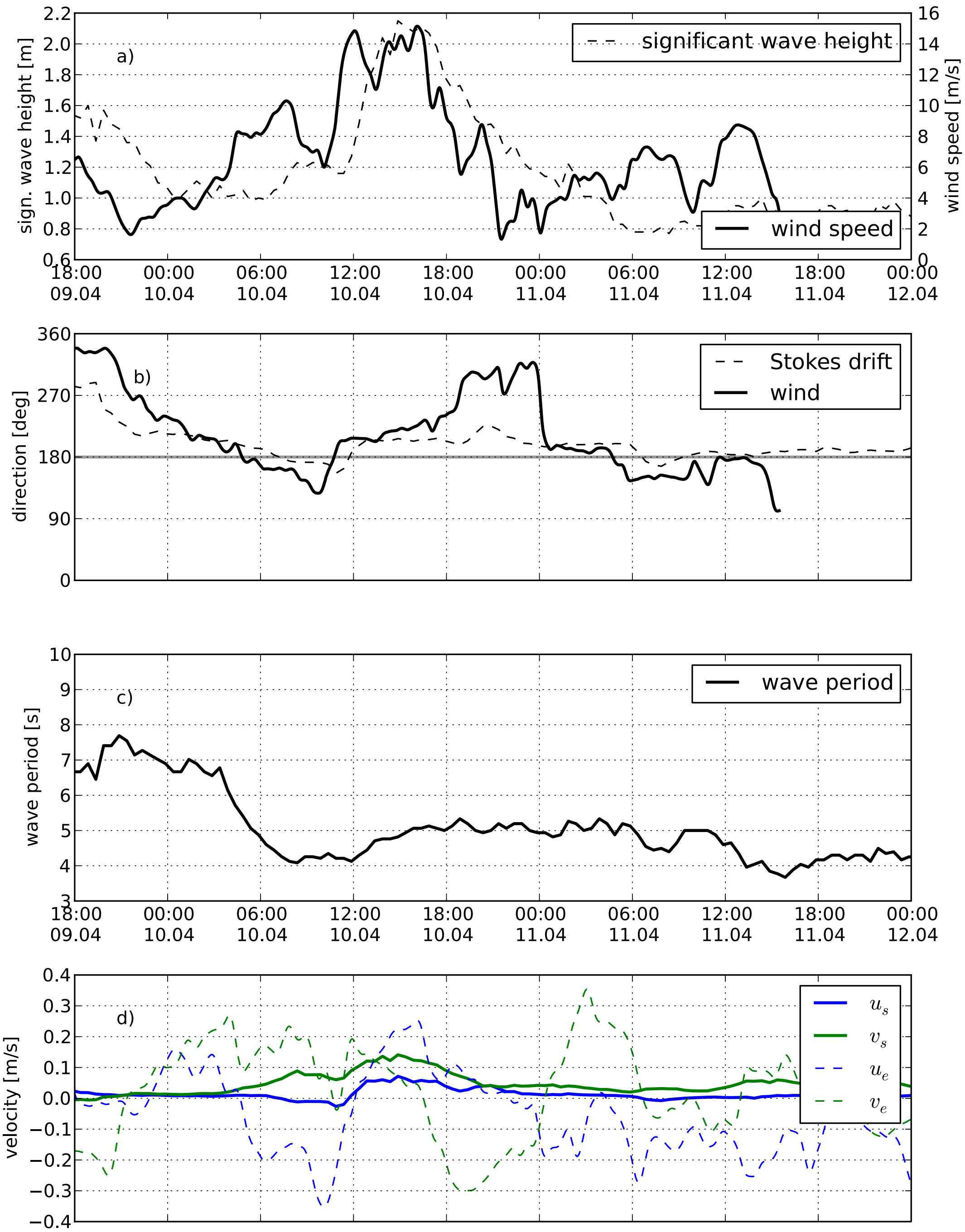

Fig. 2 Measurements at mooring station in Vestfjorden during April 9 at 1800 hours–April 12 at 0000 hours. **a** Wind speed and significant wave height. **b** Wind direction and direction of the Stokes drift at the surface. **c** Mean zero up-crossing wave period. **d** Eulerian current at 0.5-m depth (*dashed lines*) and Stokes drift at the surface (*solid lines*). Easterly and northerly components are shown, respectively

moved in from Iceland, moving northwards towards the Greenland coast. The wind direction over Lofoten changed to south–southwest with 8 m/s by 0600 hours on April 10 (Fig. 2a, b). As the low pressure system deepened and moved further northwards, the wind picked up to a maximum of 15 m/s while the direction remained rather constant.

Waves were governed by the prevailing southwesterly winds, and the significant wave height was up to 1.5 m at the experiment site (Fig. 2a, b). Figure 2c shows long wave periods before April 10 at 0600 hours, hence some swell was entering Vestfjorden. As the wind picked up from the south, the Lofoten peninsula no longer acted to shelter the waves and the significant wave height picked up to become 2.2 m at about 1400 hours on April 10 at the experiment site. After this event, the significant wave height declined slowly as the wind ceased. The wave period was constant in the decay phase, and it is likely that some swell is present in the decay period.

4.2 Ocean circulation

The general ocean circulation during the cruise is in agreement with the historically observed circulation pattern. Vertical averaged ADCP data show a dominant current towards southwest. This is consistent with the cyclonic eddy reported by Michelson-Jacob and Sundby (2001), being located in its northwestern segment. This eddy is typically dominating the circulation in Vestfjorden.

A harmonic analysis of ADCP currents was performed using the software of Pawlowicz et al. (2002). Tidal motion, whose major constituent is the lunar component M2, is limited to the zonal velocities of the barotropic current. Spectral analysis of upper ocean currents above 10-m depth show peaks at 13.1 ± 1.0 h. This peak is close to the tidal period $T_{\mathrm{M2}} = 12.4$ h as well as to the inertial period $T_{\mathrm{int}} = 12.9$ h. A transient signal with such a period in the ADCP data shows an upward propagating internal wave phase. This implies downward propagating energy, which means that the wave is generated at the surface (Alford and Gregg 2001), most likely during the strong winds on April 10 (Fig. 2a). This wind event created an inertial oscillation, which is also evident from the drifter data where it appears as anticyclonic loops in the trajectories (Fig. 1).

Measured surface currents and Stokes drift during the experiment are shown in Fig. 2d. Components of Eulerian current at 0.5-m depth are shown; this is the uppermost layer that could be observed by the ADCP. The Stokes drift at the surface (0-m depth) is calculated from the measured directional wave spectra according to Eq. 5. Throughout the experiment, the magnitude of the Stokes drift is on average 20 % of the Eulerian current. During the wind event on the 10th of April, between 1200 hours and 1800 hours, the Stokes drift even reaches the same magnitude as the Eulerian current. Notably, the Stokes drift has a rather unidirectional behaviour, while the Eulerian current exhibits much more high-frequency variations. As for example, the inertial oscillation described above appears as strong perturbation on April 10 and April 11 in both components of the Eulerian current.

5 Analysis of drifter and wave buoy data

5.1 Drifter deployments

Two types of drifters were deployed to study differences in their behaviour and to compare their drift with observed geophysical fields. Drifters were released 5 km close to the mooring triangle. The iSpheres stayed within 14-km distance to the moorings; their trajectories are related to ADCP currents and the wave field in Section 5.4.

Unintentionally, the SLDMB drifters moved away from the moorings. Located at 1-m depth, they followed the general current pattern southwestwards, as described in Section 3.1. Contrary, the iSpheres at 0-m depths moved somewhat with wind and waves towards north as expected (Fig. 1).

Time series of average drifter speeds for the two drifter types demonstrate their different response to wind events (Fig. 3). Prior to the onset of the wind early April 10, both drifter types had comparable speeds and both were drifting towards southwest (Fig. 1, first deployment). The wind then increased, and the iSpheres

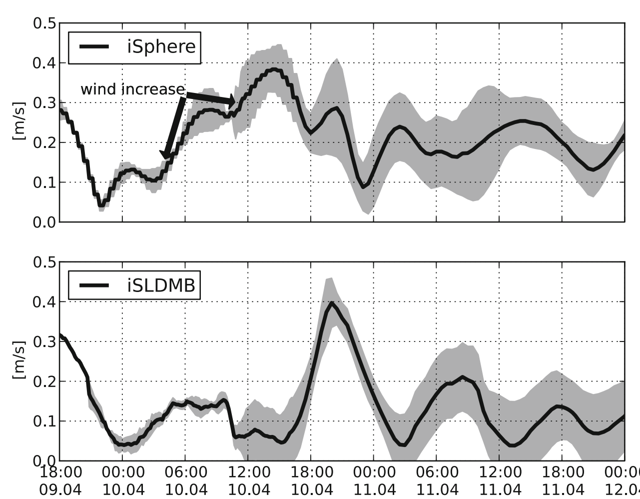

Fig. 3 Drifter speed during April 9 at 1800 hours–April 12 at 0000 hours. The *upper graph* shows average speed of iSphere drifters, the shading shows standard deviation. The *lower graph* shows the same for the SLDMBs. Average and standard deviation was calculated from zonal and meridional components of the drifters and then transferred to absolute speeds

turned rapidly and started to drift approximately in the wind direction. The SLDMBs did not immediately respond to the wind event. About 12 h later, after the wind has set up inertial currents, the SLDMBs speed went up as well.

The second deployment included four drifters of each type that were released southeast of the mooring triangle with about one nautical mile between the pairs (Fig. 1). The SLDMBs rapidly aligned along the steep slope drifting towards south-west, while the iSpheres drifted northwards in wind and wave direction.

5.2 Structure of geophysical forcing

More details on the different behaviour of the two drifter types were obtained from the present data. To estimate the spatial scales of their geophysical forcing fields, we follow an analysis similarly performed by Davis (1985b), who calculated correlations between drifter pairs as a function of their separation.

We split up all drifter trajectories in pieces of 3 h. Correlation coefficients of simultaneous pairs of 3-h trajectories were then calculated from drifter velocities. Different from Davis' analysis, we use the following definition of a vector correlation:

$$r = 1 - \frac{<(\mathbf{v}_i - \mathbf{v}_j)^2>}{<\mathbf{v}_i^2> + <\mathbf{v}_j^2>}, \tag{11}$$

The correlation coefficient r becomes equal to one for identical velocities and minus one for opposite velocities. Separation distances for each pair were calculated and divided into 1-km bins. Correlation coefficients in the same bin were averaged, yielding an average correlation as a function of separation. This result is shown in Fig. 4 for each drifter type separately. Some SLDMB drifter data are available after the duration of this experiment because the drifters stayed in Vestfjorden. Drifter data up until the 14th of April have been used in this analysis. Figure 4 also shows correlations between SLDMB drifters and the Lagrangian current measured at the mooring station, which was calculated from ADCP and waverider data following Eq. 3.

Average correlations between pairs of iSphere drifters remain above 0.8 up until 10-km separation distance. The SLDMB drifters decorrelate rapidly in the beginning, after only 5 km the average correlations drop below 0.6. The iSphere drifters stay correlated as they separate, which indicates that their forcing exhibits large horizontal scales.

The iSphere drifters are located directly at the air–sea interface, their drift velocity is largely driven by

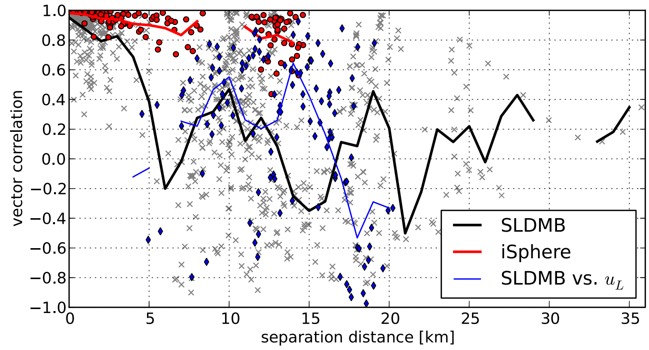

Fig. 4 Vector correlations between drifter pairs as a function of separation distance. The *points* show individual correlations and the *lines* show bin averages. The *blue line* and the *blue diamonds* show correlations between SLDMB drifters and Eulerian currents measured at the mooring station, which is given by the sum of ADCP currents and the Stokes drift

wind and waves. The current further down is to a larger extent influenced by the mesoscale and submesoscale variability of the ocean circulation, as resembled by the SLDMBs.

The SLDMBs follow the current at 1-m depth (Davis 1985a); their velocities can therefore be used to infer statistics of the current. From the decorrelation of SLDMB drifters, we therefore deduct that the spatial scale of the current at 1-m depth is about 5–10 km, after which their average correlation drops below 0.5.

5.3 Estimated wave-induced forcing of ocean currents

In this section, we will evaluate the wave-forcing on the Eulerian current. The direct effect of waves on drifters is evaluated in the next section. As with indirect wave effect, we refer to the fact that the drifters are advected by the Eulerian current $\mathbf{u}_\mathrm{E}$, which itself is modified by waves as described in Section 2.3.

The Eulerian current that is measured by the ADCP includes the part of the current that is due to wave-induced surface fluxes and the Coriolis–Stokes force. An ocean model attempts to model the Eulerian current, but these wave effects are most commonly not included. Estimates of the wave-induced forcing have been obtained from measured wave spectra. The values of the source terms in the integrals of Eqs. 6 and 9 have been calculated using the formulations given in Chapter 3.3 of Komen et al. (1994). These are also used in the wave model WAM, as implemented at the Norwegian Meteorological Institute.

The Eulerian current is also forced by winds: the total atmospheric momentum flux $\boldsymbol{\tau}_a$ has been calculated from observed wind speed and the bulk flux formula by using the values in Smith (1988). The energy fluxes from wind and waves have been estimated according to Eqs. 7 and 8, respectively.

In Fig. 5a, we see how the ratio between the effective ocean surface stress τ_o and the total atmospheric flux τ_a changes with wind and waves conditions. In rising winds, the short wind-waves grow rapidly and a larger fraction of the atmospheric flux goes into the wave field instead to the mean ocean currents. In falling winds, we see that this situation is reversed; the low wind speeds yield a weak atmospheric flux, but the developed wave field now provides a comparatively strong source of mean momentum through wave dissipation processes. These results are in agreement with studies based on wave model runs (Weber et al. 2006; Saetra et al. 2007), which shows that the discrepancy between the total atmospheric flux and the effective ocean surface stress is frequently between 20 and 30 %. In Fig. 5b, we show the energy fluxes into and out of the wave field; these are atmospheric fluxes transferred into wave energy and wave energy transferred to oceanic TKE. We see that the fluxes are not perfectly balanced. The influx is larger than the outflux, hence the waves take up energy and transport it away from the measurement location. Also shown is the parametrisation of Craig and Banner (1994), which is often used to model the TKE flux to the ocean due to breaking waves. The parametrisation is quite good, although it is better correlated with the influx to the waves than the outflux from the waves to the ocean. During the wind event, the flux of TKE to the ocean increased substantially, which caused increased levels of upper ocean turbulence and a deepening of the mixed layer. Such processes are important to model correctly as the effective eddy viscosity determines how momentum is distributed in the water column and thus how the upper ocean currents develop in response to external forcing by wind and waves.

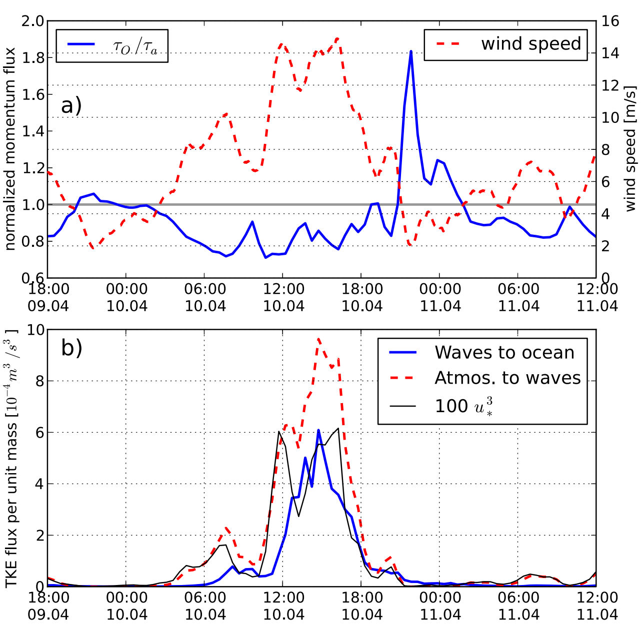

Fig. 5 **a** Momentum fluxes. The *solid line* shows the momentum flux into the ocean normalised by the total atmospheric flux. The *dashed line* shows the wind speed. **b** Energy fluxes into and out of the wave field. The *thin black line* shows the parametrisation of Craig and Banner (1994), which is frequently used to model TKE flux due to breaking waves

Another aspect of wave-induced forcing of the Eulerian current is the Coriolis–Stokes force (Eq. 10), which is given by the Stokes drift in the upper 1 m derived from the measured wave spectra, Eqs. 5, and 10. The Coriolis force due to the Eulerian mean current is $-\rho_w f\mathbf{k} \times \mathbf{u}_{\mathrm{E}}$. Hence, the relation between the Coriolis–Stokes force and the standard Coriolis force is given by the relation between the Stokes drift and the Eulerian current. Both are shown in Fig. 2d. During strong wind and high waves, as during April 10 and 11, the Coriolis–Stokes force is as much as 80 % of the standard Coriolis force. During the time scale of one inertial period, this might alter the direction of the upper ocean current by several deca-degrees as shown by Polton et al. (2005).

5.4 Wave effects on drifter trajectories

Our observations of the Eulerian current from the ADCP include the wave-forcing effects on currents that were described in the previous section. Additionally, surface drifters are also direct subject to the Stokes drift. In order to evaluate the drifter trajectories in terms of their forcings, we formulate a drift model that is based on Eq. 1 and observations of Eulerian currents, waves and wind.

Because we only have Eulerian observations at one point, we assume horizontal constant geophysical fields within 7 km around our observations. This may be justified by the analysis in Section 5.2 which shows that the forcing of iSphere drifters exhibit horizontal scales larger that this. Figure 4 shows that the iSphere drifters remained highly correlated up until the separation distances of 15 km. Our iSphere drifters stayed within a radius of 7 km around the measurement site for 2 days.

The deployment of the SLDMBs did not succeed as they immediately drifted away from the site (see Fig. 1). Spatial scales of the current that are forcing the SLDMBs were found to be at about 5–10 km. We cannot assume that our Eulerian measurements at 1-m depth are representative for a wider area. Hence, the following analysis only considers the iSpheres.

5.4.1 An analytical solution of the drift equation

We evaluate the equation of motion (Eq. 1) for the iSphere drifters, neglecting the Coriolis force $\mathbf{F}_{\mathrm{C}}$, wave scattering F_w and the drifter's inertia, hence removing the acceleration term. Now Eq. 1 becomes

$$\mathbf{F}_a + \mathbf{F}_o = 0, \tag{12}$$

stating that the drifter motion is balanced by atmospheric and ocean drag forces. We express the atmospheric drag in the same way as the oceanic drag using the wind speed $U_{19.5}$ (our winds were measured at 19.5 m high during the cruise). Since the drifter velocities are generally much smaller than the wind speed, we have approximately

$$\mathbf{F}_a = \frac{1}{2}\rho_a A_a C_a |\mathbf{U}_{19.5}|\mathbf{U}_{19.5}. \tag{13}$$

From Eqs. 2, 12 and 13 we obtain

$$-\left|\mathbf{u}_{\mathrm{L}} - \frac{\mathrm{d}\mathbf{x}}{\mathrm{d}t}\right|\left(\mathbf{u}_{\mathrm{L}} - \frac{\mathrm{d}\mathbf{x}}{\mathrm{d}t}\right) = \alpha^2\,|\mathbf{U}_{19.5}|\,\mathbf{U}_{19.5}; \tag{14}$$

$$\alpha = \sqrt{\frac{\rho_a}{\rho_w}\frac{A_a}{A_w}\frac{C_a}{C_w}}. \tag{15}$$

The equation governing the drifter motion becomes

$$\frac{\mathrm{d}\mathbf{x}}{\mathrm{d}t} = \mathbf{u}_{\mathrm{L}} + \alpha\mathbf{U}_{19.5}. \tag{16}$$

We rederive the force balance (Eq. 14) from Eq. 16 by writing Eq. 16 as

$$\alpha\mathbf{U}_{19.5} = \mathbf{s} \tag{17}$$

with $\mathbf{s} = -(\mathbf{u}_{\mathrm{L}} - \frac{\mathrm{d}\mathbf{x}}{\mathrm{d}t})$. Multiplying Eq. 17 with its scalar equivalent, i.e. $\alpha|\mathbf{U}_{19.5}| = |\mathbf{s}|$, yields Eq. 14.

5.4.2 Evaluation of drifter models

We will now evaluate the performance of four different drift trajectory models. The first is based on the force balance described in Section 5.4.1, while the others are simplified versions of this model. In one model, the Stokes drift will be totally neglected and another model parameterizes the Stokes drift as a function of wind velocity. Further models neglect wind drift, using either the Eulerian or Lagrangian current.

Equations 16 and 3 are used to define a "Lagrangian leeway model", which takes observations of wind, waves and currents into account:

$$\frac{\mathrm{d}\mathbf{x}}{\mathrm{d}t} = \mathbf{u}_{\mathrm{E}} + \mathbf{u}_{\mathrm{S}} + \alpha\mathbf{U}_{19.5}, \tag{18}$$

If one neglects waves, say $\mathbf{u}_{\mathrm{L}} \approx \mathbf{u}_{\mathrm{E}}$, Eq. 18 becomes

$$\frac{\mathrm{d}\mathbf{x}}{\mathrm{d}t} = \mathbf{u}_{\mathrm{E}} + \alpha\mathbf{U}_{19.5} \tag{19}$$

This model will be referred to as "Eulerian leeway model" because the drifter follows the Eulerian current with some wind drift.

It is possible to parameterize the Stokes drift by the wind, assuming that wind and waves are aligned and that the wave field is in a steady state. We define such a "Eulerian model with parameterized Stokes drift" as follows:

$$\frac{\mathrm{d}\mathbf{x}}{\mathrm{d}t} = \mathbf{u}_{\mathrm{E}} + \beta\mathbf{U}_{19.5}; \tag{20}$$

$$\beta = \alpha + \frac{|\mathbf{u}_s|}{|\mathbf{U}_{19.5}|} \tag{21}$$

Here, the parameter β includes the drift by surface waves. The two different parameters α and β are estimated empirically in the following analysis. We did not calculate α directly from Eq. 15 because the form drag coefficients C_a and C_w are Reynolds number dependent and are not straightforward to use at the air–sea boundary layer with wave disturbances. Rather than studying this problem in detail, this study focuses on the question which of the defined models delivers best agreement with observations.

We estimate α by fitting Eq. 18 to the observations, this yields a best guess for the present wind drag. β is found by fitting Eq. 20 to the observations and does thereby implicitly include the wave drift as good as possible. The Eulerian leeway model with wave parametrisation is therefore the best possible attempt to model a drifter without wave information.

Furthermore, two models are evaluated that neglect wind drag. Equation 18 then reduces to

$$\frac{\mathrm{d}\mathbf{x}}{\mathrm{d}t} = \mathbf{u}_{\mathrm{E}} + \mathbf{u}_{\mathrm{S}}, \tag{22}$$

say the drifter simply follows the Lagrangian current; herein referred to as "Lagrangian model". The last

Table 2 Models for drifter velocity, wind drag parameters α (or β if applicable), and respective skill scores for different time periods and averages for the entire experiment

	Drifter velocity	α / β	Case a	Case b	Case c	Case d	Average
Eulerian model	$dx/dt = u_E$		0.66	0.39	0.59	0.54	0.55
Lagrangian model	$dx/dt = u_L$		0.6	0.74	0.83	0.67	0.72
Eulerian leeway model	$dx/dt = u_E + \alpha U_{19.5}$	3.1e–3	0.63	0.47	0.65	No data	0.60
Eulerian leeway model with wave parametrisation	$dx/dt = u_E + \beta U_{19.5}$	9.9e–3	0.56	0.65	0.74	No data	0.67
Lagrangian leeway model	$dx/dt = u_L + \alpha U_{19.5}$	3.1e–3	0.56	0.83	0.85	No data	0.77

model, referred to as the "Eulerian model", neglects both wind and waves:

$$\frac{d\mathbf{x}}{dt} = \mathbf{u}_E \tag{23}$$

All four models are summarised in Table 2. We can now evaluate the different models based on our observations. Eulerian currents are taken from the ADCP measurements in 0.5-m depth, which is the uppermost layer that the ADCP could measure. The Stokes drift is obtained from the wave rider buoy using Eq. 5. The wind is given at 19.5 m above sea surface.

With the given measurements, the drifter velocities of each model from Eqs. 18–23 are integrated numerically with 2-min steps. The integration yields paths of modelled drifter trajectories, shown in Fig. 6 for an example period with considerably strong waves. Additionally, an average path of all drifters during the same period is shown. In this figure, all trajectories start at the same point in order to compare their paths.

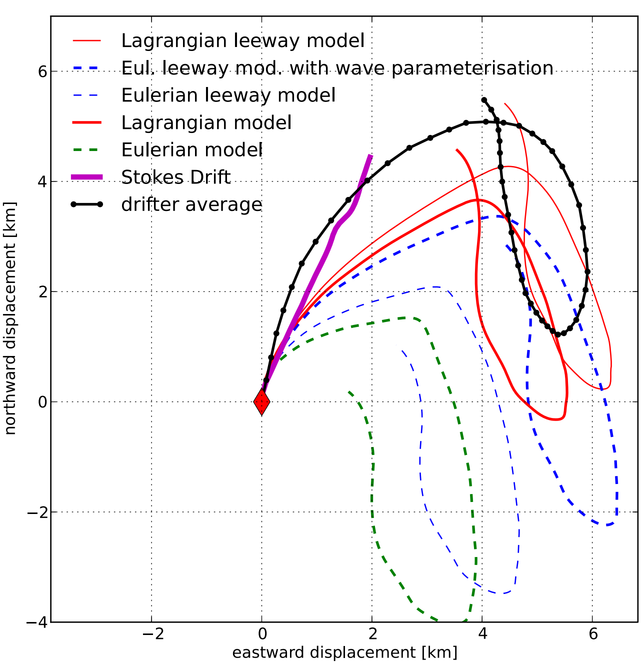

Fig. 6 Integrated velocities of the four drifter models and the Stokes drift from April 10 at 1200 hours to April 11 at 0600 hours; the *black line with dots* is an average path of all iSphere drifters during this time. Starting points (*red diamond*) have been put together to compare the different paths

The models that involve wave observations (red lines) do generally show better agreement with the drifter average (black line) than the models without wave information (blue and green lines), even though the Eulerian leeway model with wave parametrisation includes wave drift implicitly by a larger wind drag parameter β.

The agreement of each model with the observed trajectories is evaluated using a separation metric that yields a skill score for each model. As separation metric, the normalised cumulative Lagrangian separation suggested by Liu and Weisberg (2011) is applied. This procedure gives a separation s between a modelled and a observed trajectory:

$$s = \sum d_i \Big/ \sum_{i=0}^{N} \sum_{j=0}^{i} dl_j \tag{24}$$

The indices $i, j = 0, ..., N$ denominate measurements along a trajectory, d_i are distances between the modelled and observed positions, and dl_j are distances between the current and the last position on the observed trajectory. Positions on two minute steps are used, while drifter positions are interpolated to these steps. A skill score ss is defined as

$$ss = \begin{cases} 1 - s & \text{if} \quad s \leq 1 \\ 0 & \text{if} \quad s > 1 \end{cases} \tag{25}$$

This definition of a skill score by Liu and Weisberg (2011) evaluates the entire trajectory cumulative. High skill scores close to one mean good agreement between model and observation throughout the entire trajectory. The parameters α and β are estimated by optimising the average skill score for all iSphere drifters during the entire experiment from April 9 at 1800 hours to April 12 at 0000 hours. Results are given in Table 2.

Beside average skill scores for the entire experiment and all drifters, Table 2 also shows skill scores for shorter time periods. The entire data set of iSphere

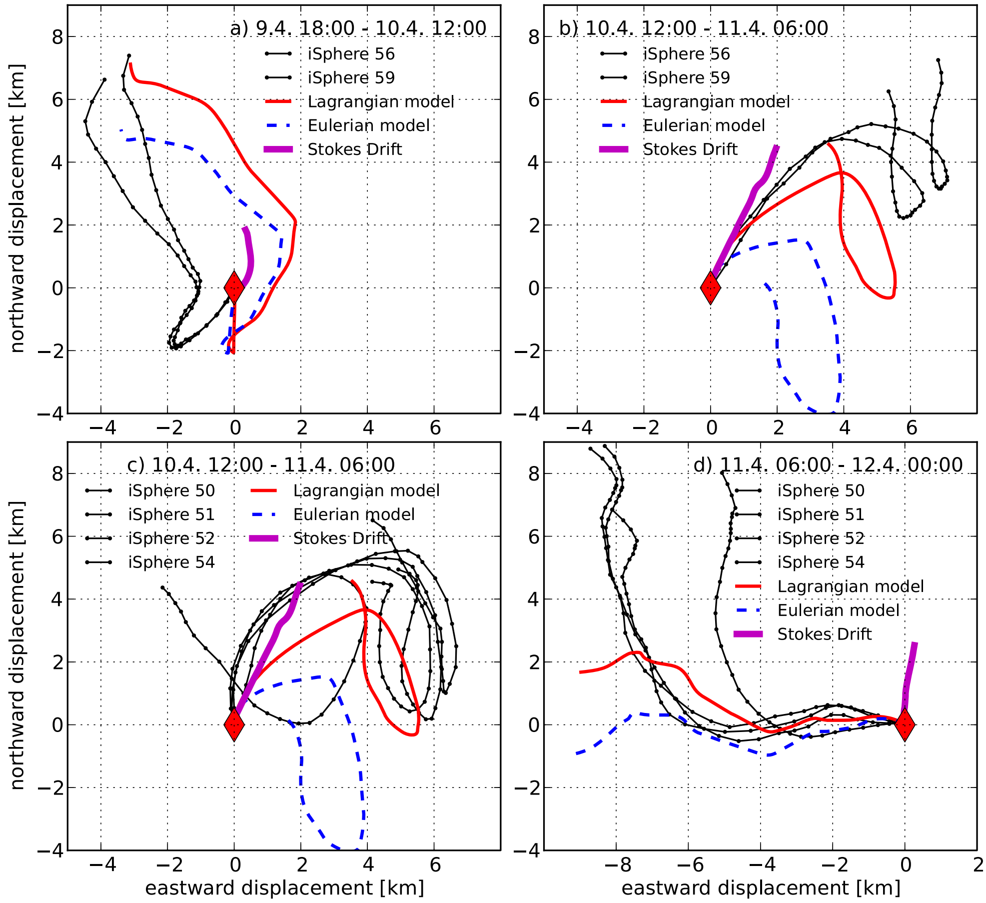

Fig. 7 Integrated velocities of the Eulerian drift model, the Lagrangian drift model and the Stokes drift for four different 18-h cases. The *black lines* with dots shows trajectories of iSphere drifters. **b** and **c** show the same time period with different drifters

drifters is split up in 18-h periods; individual drifter trajectories for these periods are plotted in Fig. 7.

During case a, accounting for wave information does not enhance the model significantly as the skill score for case a is not raised. During this period, the significant wave height is rather moderate (compare Fig. 2a), and the integrated Stokes drift yields a rather short path (Fig. 7a). Adding wave information does not change much when waves are small.

During the following periods, however, waves are stronger and contribute significantly to the trajectories. Skill scores for the Eulerian model are raised from 0.55 to 0.72 in the Lagrangian model, in which the Stokes drift is added to the drifter velocity. The Eulerian leeway model with wave parametrisation takes the forward motion from waves implicitly into account because an empirical parameter is used here to suit the observations. Taking the Stokes drift properly into account, which is done in the Lagrangian leeway model, still enhances the skill score from 0.67 to 0.77.

The Eulerian leeway model with wave parametrisation fails if the waves are not aligned with the wind. This is the case on April 10, as shown in Fig. 2b. The discrepancy in directions can only be accounted for when a wave model is used in trajectory forecasts.

It is furthermore worth to point out that the Lagrangian leeway model is less sensitive to inaccuracies in the parameters α and β because the wind drag accounts for a smaller fraction of the drifter velocities when the Stokes drift is used explicitly. The parameter β for the Eulerian model parametrises the Stokes drift and the wind drag. The parameter α for the Lagrangian model only accounts for wind drag. Their difference thus represents the wave drift by wind speed. The present observations show $\beta \approx 3\alpha$. Conclusively, the Stokes drift is twice as large as the wind drag for the used iSphere drifters.

6 Summary and concluding remarks

We have shown results from a research cruise during April 2011 in Vestfjorden, northern Norway. The observations include Eulerian currents, wave spectra, wind speed and direction, and drifter trajectories. Observed drift trajectories were reconstructed by drift models based on observations.

Drift models were formulated with and without wind drag, as well as with and without wave information. Two types of wind drag parameters were obtained empirically: one that only accounts for the pure wind drag and one that also parametrises the Stokes drift. The trajectories of the surface drifting iSpheres were well reconstructed by the Lagrangian mean currents, that is when wave information are used. It was shown that the Stokes drift accounted for twice as much drift compared to the wind drag for the given surface drifter. These results are specific for drifters located directly at the air–sea interface. The findings from the iSphere drifters do particularly not apply to water following drifters below the surface.

Wave-induced surface fluxes and the Coriolis–Stokes force could be calculated from the present measurements. Their impact in terms of difference in current, however, could not be quantified with measurements because such calculations require the time-integration of the momentum equations. This can be done with a coupled model system of waves and ocean currents as described by Broström et al. (2008).

For the computation of the Stokes drift, we do not know exactly how the wave buoy responds to short waves and how much energy that is contained in the tail of the wave spectrum. In numerical wave prediction models the spectral tail is parametrised. The formulation of the Stokes drift (Eq. 5) is proportional to the third moment of the wave frequency spectrum and is therefore sensitive to formulation of the spectral tail.

We suggest that the predictability of drift trajectories can be improved by adding wave information from a numerical wave model. First of all, it is important to have reliable estimates of the Stokes drift, which has comparable magnitudes to the Eulerian mean current during strong wind events. Second, the wave-induced fluxes of momentum and energy, and the Coriolis–Stokes force, are all significant and are likely to be important for the development of the Eulerian mean current. The drift trajectories of the submerged drifters reflect the small scale variability related to eddies, inertial oscillations, tides and so on. Hence, prediction of these trajectories strongly depends on the performance of the ocean model.

Good estimates of the effective eddy viscosities are necessary to realistically model the current shear and surface velocities. Wave-induced turbulence is an active field of research, and there is currently no consensus how such processes should be incorporated in ocean models. Progress in this field has to some extent been hampered by the lack of reliable turbulence measurements in the upper layer of the ocean. In contrast, both the Stokes drift, the wave dependent air–sea fluxes and the Coriolis–Stokes force are readily included in some current ocean modelling systems. All that is required is a numerical wave model that can provide the necessary directional wave spectra and algorithms for calculating the Stokes drift and the forcing fields.

The forecast skill of a numerical wave model is usually on par with the skill of the atmospheric forecast model that provides the wind forcing. The forecast skill of ocean models is usually much lower than this due to small scale variability that is not properly resolved. In particular, the ocean currents are difficult to predict. Each added wave "feature" will therefore help reduce the uncertainties in the prediction of drift trajectories.

Acknowledgements We wish to thank Ilker Fer and Øyvind Sætra for helpful discussions. We also gratefully acknowledge financial support from the Research Council of Norway through the grants 196438 (BioWave) and 207541 (OilWave), as well as the Gulf of Mexico Research Initiative Deep-C Consortium. We also thank the Royal Norwegian Navy for supplying us with the ADCP instrument, as well as Steinar Hansen from the Norwegian Coastal Administration for providing necessary logistics. We are grateful for the constructive comments of the anonymous reviewers, who helped to increase the quality of this paper significantly.

References

Aamo OM, Jensen H (1997) Operational use of ocean surface drifters for tracking spilled oil. In: Proceedings of the 20th Arctic and Marine Oil Spill Program (AMOP) technical seminar, Vancouver, Canada

Alford MH, Gregg MC (2001) Near-inertial mixing: modulation of shear, strain and microstructure at low latitude. J Geophys Res 106(C8):16947–16968. doi:10.1029/2000JC000370

Ardhuin F, Marie L, Rascle N, Forget P, Roland A (2009) Observation and estimation of Lagrangian, Stokes, and Eulerian currents induced by wind and waves at the sea surface. J Phys Oceanogr 39(11):2820–2838. doi:10.1175/2009JPO4169.1

Belore R, Trudel K, Morrison J (2011) Weathering, emulsification, and chemical dispersibility of Mississippi Canyon 252 crude oil: field and laboratory studies. In: 2011 international oil spill conference. Portland, Oregon

Breivik O, Allen AA (2008) An operational search and rescue model for the Norwegian Sea and the North Sea. J Marine Syst 69(1–2):99–113. doi:10.1016/j.jmarsys.2007.02.010

Breivik O, Allen AA, Maisondieu C, Roth J (2011) Wind-induced drift on objects at sea: the leaway field method. Appl Ocean Res 33:100–109. doi:10.1016/j.apor.2011.01.005

Broström G, Christensen KH, Weber JEH (2008) A quasi-Eulerian, quasi-Lagrangian view of surface-wave-induced flow in the ocean. J Phys Oceanogr 38(5):1122–1130. doi:10.1175/2007JPO3702.1

Carniel S, Warner J, Chiggiato J, Sclavo M (2009) Investigating the impact of surface wave breaking on modeling the trajectories of drifters in the northern Adriatic Sea during a wind-storm event. Ocean Model 30(2–3):225–239. doi:10.1016/j.ocemod.2009.07.001

Craig PD, Banner ML (1994) Modeling wave-enhanced turbulence in the ocean surface layer. J Phys Oceanogr 24(12): 2546–2559. doi:10.1175/1520-0485(1994)024<2546:MWETIT>2.0.CO;2

Craik ADD (1982) The drift velocity of water waves. J Fluid Mech 116:187–205. doi:10.1017/S0022112082000421

Craik ADD, Leibovich S (1976) Rational model for Langmuir circulations. J Fluid Mech 73:401–426. doi:10.1017/S0022112076001420

Daniel P, Jan G, Cabioc'h F, Landau Y, Loiseau E (2002) Drift modeling of cargo containers. Spill Sci Technol B 7(5–6):279–288. doi:10.1016/S1353-2561(02)00075-0

Datawell (2007) Datawell waverider reference manual. Technical report, Datawell BV. www.datawell.nl. Accessed 20.09.2011

Davis RE (1985a) Drifter observations of coastal surface currents during code: the method and descriptive view. J Geophys Res 90(C3):4741–4755. doi:10.1029/JC090iC03p04741

Davis RE (1985b) Drifter observations of coastal surface currents during code: the statistical and dynamical views. J Geophys Res 90:4756–4772. doi:10.1029/JC090iC03p04756

Emery W, Thomson RE (1997) Data analysis methods in physical oceanography. Elsevier, Amsterdam

Grant ALM, Belcher SE (2009) Characteristics of Langmuir turbulence in the ocean mixed layer. J Phys Oceanogr 39(8):1871–1887. doi:10.1175/2009JPO4119.1

Janssen PAEM (1989) Wave-induced stress and the drag of air flow over sea waves. J Phys Oceanogr 19:745–754

Jenkins AD (1989) The use of a wave prediction model for driving a near-surface current model. Ocean Dyn 42:133–149. doi:10.1007/BF02226291

Jones B, Boudjelas S, Michelson-Jacob E (1997) Topographic steering of winds in vestfjorden. Weather - London 52(10): 304–311

Komen GJ, Cavaleri L, Doneland M, Hasselmann K, Hasselmann S, Janssen PAE (1994) Dynamics and modelling of ocean waves. Cambridge University Press, Cambridge

Liu Y, Weisberg RH (2011) Evaluation of trajectory modeling in different dynamic regions using normalized cumulative Lagrangian separation. J Geophys Res 116(C9):C09013. doi:10.1029/2010JC006837

Longuet-Higgins MS (1953) Mass transport in water waves. Philos Trans R Soc 245:535–581

Longuet-Higgins M, Stewart R (1964) Radiation stress in water waves; a physical discussion with applications. Deep-Sea Res 11:529–562. doi:10.1016/0011-7471(64)90001-4

Michelson-Jacob G, Sundby S (2001) Eddies of Vestfjorden, Norway. Cont Shelf Res 21(16–17):1901–1918. doi:10.1016/S0278-4343(01)00030-9

O'Donnell J, Allen A, Murphy D (1997) An assessment of the errors in lagrangian velocity estimates obtained by fgge drifters in the Labrador current. J Atmos Ocean Technol 14(2): 292–307. doi:10.1175/1520-0426(1997)014<0292:AAOTEI>2.0.CO;2

Pawlowicz R, Beardsley B, Lentz S (2002) Classical tidal harmonic analysis including error estimates in Matlab using t_tide. Comput Geosci 28(8):929–937. doi:10.1016/S0098-3004(02)00013-4

Perrie W, Tang CL, Hu Y, DeTracy BM (2003) The impact of waves on surface currents. J Phys Oceanogr 33(10):2126–2140. doi:10.1175/1520-0485(2003)033<2126:TIOWOS>2.0.CO;2

Phillips OM (1977) The dynamics of the upper ocean. Cambridge University Press, London

Polton JA, Lewis DM, Belcher SE (2005) The role of wave-induced Coriolis–Stokes forcing on the wind-driven mixed layer. J Phys Oceanogr 35(4):444–457. doi:10.1175/JPO2701.1

Rascle N, Ardhuin F (2009) Drift and mixing under the ocean surface revisited: stratified conditions and model-data comparisons. J Geophys Res 114(C2):C02016. doi:10.1029/2007JC004466

Roed L (1980) Curvature effects on hydraulically driven inertial boundary currents. J Fluid Mech 96(2):395–412. doi:10.1017/S0022112080002182

Saetra Ø, Albretsen J, Janssen PAEM (2007) Sea-state-dependent momentum fluxes for ocean modeling. J Phys Oceanogr 37(11):2714–2725. doi:10.1175/2007JPO3582.1

Smith S (1988) Coefficients for sea surface wind stress, heat flux, and wind profiles as a function of wind speed and temperature. J Geophys Res 93(C12)(2):311–326. doi:10.1016/0021-9991(88)90175-1

Stokes GG (1847) On the theory of oscillatory waves. Trans Camb Philos Soc 8:441–473

Sundby S (1982) Fresh water budget and wind conditions. In: Investigations in Vestfjorden 1978. ftp://ftp.imr.no/biblioteket/files/havforsk/fh_1982_01.pdf. Accessed 21.09.2011, Fisken og Havet, 1982: 16 s. [In Norwegian, English abstract]

Tang C, Perrie W, Jenkins A, DeTracey B, Hu Y, Toulany B, Smith P (2007) Observation and modeling of surface currents on the Grand Banks: a study of the wave effects on surface currents. J Geophys Res 112(C10):C10025. doi:10.1029/2006JC004028

Weber J, Broström G, Saetra O (2006) Eulerian vs Lagrangian approaches to the wave-induced transport in the upper ocean. J Phys Oceanogr 36:2106–2118. doi:10.1175/JPO2951.1

Weber J, Broström G, Christensen K (2008) Radiation stress and depth-dependent drift in surface waves with dissipation. Int J Offshore Polar 18(1):8–13

Weber JE (1983) Steady wind- and wave-induced currents in the open ocean. J Phys Oceanogr 13(3):524–530. doi:10.1175/1520-0485(1983)013<0524:SWAWIC>2.0.CO;2

Weber JE, Christensen KH, Denamiel C (2009) Wave-induced set-up of the mean surface over a sloping beach. Cont Shelf Res 29:1448–1453. doi:10.1016/j.csr.2009.03.010